



Tel2 structure and function in the Hsp90-dependent maturation of mTOR and ATR complexes

Hiroyuki Takai, Yihu Xie, Titia de Lange, et al.

Genes Dev. 2010 24: 2019-2030 originally published online August 27, 2010

Access the most recent version at doi:[10.1101/gad.1956410](https://doi.org/10.1101/gad.1956410)

**Supplemental
Material**

<http://genesdev.cshlp.org/content/suppl/2010/08/19/gad.1956410.DC1.html>

References

This article cites 50 articles, 16 of which can be accessed free at:
<http://genesdev.cshlp.org/content/24/18/2019.full.html#ref-list-1>

**Email alerting
service**

Receive free email alerts when new articles cite this article - sign up in the box at the top right corner of the article or [click here](#)

To subscribe to *Genes & Development* go to:
<http://genesdev.cshlp.org/subscriptions>

Tel2 structure and function in the Hsp90-dependent maturation of mTOR and ATR complexes

Hiroyuki Takai,^{1,5} Yihu Xie,^{2,3,5} Titia de Lange,^{1,7} and Nikola P. Pavletich^{2,4,6}

¹Laboratory for Cell Biology and Genetics, The Rockefeller University, New York, New York 10065, USA; ²Structural Biology Program, Sloan-Kettering Institute, Memorial Sloan-Kettering Cancer Center, New York, New York 10065, USA; ³BCMB Allied Graduate Program, Weill Medical College of Cornell University, New York, New York 10065, USA; ⁴Howard Hughes Medical Institute, Sloan-Kettering Institute, Memorial Sloan-Kettering Cancer Center, New York, New York 10065, USA

We reported previously that the stability of all mammalian phosphatidylinositol 3-kinase-related protein kinases (PIKKs) depends on their interaction with Tel2, the ortholog of yeast Tel2 and *Caenorhabditis elegans* Clk-2. Here we provide evidence that Tel2 acts with Hsp90 in the maturation of PIKK complexes. Quantitative immunoblotting showed that the abundance of Tel2 is low compared with the PIKKs, and Tel2 preferentially bound newly synthesized ATM, ATR, mTOR, and DNA-PKcs. Tel2 complexes contained, in addition to Tti1–Tti2, the Hsp90 chaperone, and inhibition of Hsp90 interfered with the interaction of Tel2 with the PIKKs. Analysis of *in vivo* labeled nascent protein complexes showed that Tel2 and Hsp90 mediate the formation of the mTOR TORC1 and TORC2 complexes and the association of ATR with ATRIP. The structure of yeast Tel2, reported here, shows that Tel2 consists of HEAT-like helical repeats that assemble into two separate α -solenoids. Through mutagenesis, we identify a surface patch of conserved residues involved in binding to the Tti1–Tti2 complex *in vitro*. *In vivo*, mutation of this conserved patch affects cell growth, levels of PIKKs, and ATM/ATR-mediated checkpoint signaling, highlighting the importance of Tti1–Tti2 binding to the function of Tel2. Taken together, our data suggest that the Tel2–Tti1–Tti2 complex is a PIKK-specific cochaperone for Hsp90.

[*Keywords:* Tel2; Hsp90; ATR; mTOR; PIKK; structure]

Supplemental material is available at <http://www.genesdev.org>.

Received June 4, 2010; revised version accepted July 26, 2010.

Tel2 has long been an enigmatic gene, implicated in a myriad of apparently unrelated biological processes in worms, budding yeast, and fission yeast (Hartman and Herman 1982; Lustig and Petes 1986; Lakowski and Hekimi 1996; Shikata et al. 2007). An explanation for these varied phenotypes emerged from the finding that mammalian Tel2 is required for the stability of all phosphatidylinositol 3-kinase-related protein kinases (PIKKs) (Takai et al. 2007). Tel2 associates with the PIKKs, and deletion of Tel2 from mouse embryo fibroblasts (MEFs) resulted in diminished PIKK protein levels without affecting their mRNA levels. For ATM and mTOR, the diminished protein levels were shown to be due to reduced stability of newly synthesized protein. However, the mechanism by which Tel2 affects the PIKKs was not elucidated.

The six mammalian PIKKs are a family of large proteins that consist of N-terminal helical repeat domains followed by a C-terminal phosphatidylinositol 3-kinase

(PI3K)-like domain. In five of the known PIKK family members, the PI3K-like domain acts as a Ser/Thr protein kinase (mTOR, ATM, ATR, DNA-PKcs, and SMG1), while the sixth PIKK, TRRAP, lacks kinase activity (Shiloh 2003; Abraham 2004; Bakkenist and Kastan 2004; Guertin and Sabatini 2007). The PIKKs act in diverse cellular pathways. The mTOR pathway receives a number of regulatory inputs, including amino acid levels, nutrient supply, and growth factor signaling. In response, mTOR phosphorylates proteins involved in cell size control, autophagy, cell cycle progression, and proliferation. These responses are mediated by two distinct mTOR complexes, TORC1 and TORC2, which contain a common G β L subunit, but a distinct third subunit: Raptor and Rictor, respectively (Laplante and Sabatini 2009; Ma and Blenis 2009).

The ATM, ATR, and DNA-PKcs PIKKs function in pathways involved in maintaining genomic integrity. ATM and ATR sense DNA double-strand breaks (DSBs) and stalled or collapsed replication forks, respectively, and in response they initiate a cascade of phosphorylation events that lead to cell cycle arrest, activation of transcription programs, and increased repair capacity (Harper and Elledge 2007; Branzei and Foiani 2008; Cimprich and Cortez 2008). SMG1 controls nonsense-mediated decay,

⁵These authors contributed equally to this work.

Corresponding authors.

⁶E-MAIL pavletin@mskcc.org; FAX (212) 717-3135.

⁷E-MAIL delange@mail.rockefeller.edu; FAX (212) 327-7147.

Article published online ahead of print. Article and publication date are online at <http://www.genesdev.org/cgi/doi/10.1101/gad.1956410>.

Takai et al.

phosphorylating UPF1 in response to premature stop codons in mRNAs (Nicholson et al. 2010). TRRAP regulates transcription as a component of the Tip60 histone acetyltransferase complex (Murr et al. 2007).

The folding, conformational maturation, and ligand-binding activities of a growing list of regulatory and signaling proteins require the Hsp90 chaperone protein pathway. Hsp90 assembles into an array of multiprotein complexes with additional proteins, including the Hsp70 and Hsp40 chaperones, scaffold proteins, and peptidylproline isomerases, as well as proteins that are required for specific classes of substrates, or clients (Young et al. 2001; Wandinger et al. 2008). For example, the Cdc37 cochaperone directs Hsp90 complexes to conventional Ser/Thr kinase client proteins like Akt, Raf, and Cdk4, while a set of immunophilins that includes FKBP52 and cyclophilin 40 are in Hsp90 complexes that maintain certain nuclear hormone receptors in a ligand-binding-competent conformation (Wandinger et al. 2008). Inhibition of the Hsp90 ATPase cycle can block the conformational maturation process, and can also result in the rapid degradation of the client protein. Because many of the Hsp90 clients include oncoproteins, Hsp90 inhibitors such as geldanamycin and its derivatives are being investigated for cancer therapy (Whitesell and Lindquist 2005; Gray et al. 2008). Here we report that Tel2 has features of an Hsp90 cochaperone, and that the formation of several PIKK complexes requires a concerted action of Tel2, its associated Tti1–Tti2 complex, and Hsp90.

Results

Insufficient Tel2 to bind PIKKs stoichiometrically

We determined the *in vivo* stoichiometry of Tel2, mTOR, and ATM by quantitative immunoblotting (Fig. 1A,B). The immunoblots were calibrated using relevant re-

combinant protein fragments that included the epitopes for the antibodies used. The recombinant proteins were quantified by comparison of their Coomassie staining to known quantities of bovine serum albumin (BSA), with a correction for the number of Coomassie-reactive amino acids (Lys, His, Arg) in the tested proteins and BSA. Using these calibrated standards alongside extracts from two human tumor cell lines (HeLa and the fibrosarcoma-derived cell line HTC75), the absolute abundances of the endogenous Tel2, mTOR, and ATM were estimated (Fig. 1A). The results showed that the two human tumor cell lines contained 11,000 molecules of Tel2 and 14,000–22,000 molecules of ATM. mTOR was considerably more abundant, at an estimated 80,000–200,000 copies per cell (Fig. 1B). Even excluding the four PIKKs whose abundance we did not measure, the total abundance of mTOR and ATM alone would be nine to 20 times above that of Tel2, suggesting that only a fraction of these PIKKs is in a complex with Tel2 at any one time. This result is consistent with the low recovery of PIKKs in Tel2 immunoprecipitations (IPs) (Takai et al. 2007).

The Tel2–Tti1–Tti2 complex contains molecular chaperones

Proteomic analysis in fission yeast identified two specific Tel2-interacting partners, referred to as Tti1 and Tti2 (Hayashi et al. 2007; Shevchenko et al. 2008). The human orthologs of Tti1 and Tti2 (GeneID: 9675 and 80185, respectively) were also detected by our proteomic analysis of the human Tel2 complex (Fig. 1C; Supplemental Fig. 1). To further analyze the Tel2 complex, Tel2, Tti1, and Tti2 were expressed as N-terminally Flag-[HA]2-tagged proteins in HeLa S3 cells, and associated proteins were captured through sequential anti-Flag and anti-HA IPs. MALDI-TOF mass spectrometric analysis of the associated proteins confirmed the interaction of Tel2

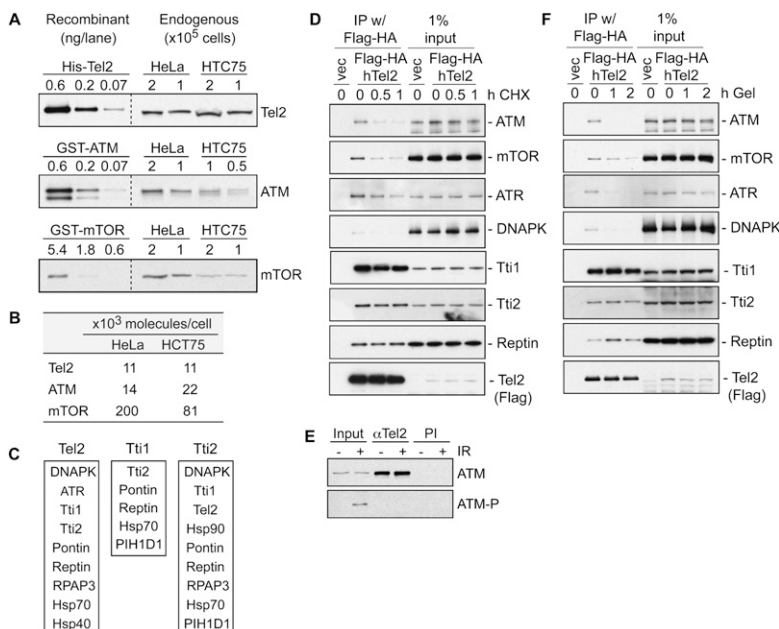


Figure 1. Tel2 binds newly synthesized PIKKs in an Hsp90-dependent manner. (A) Quantitative immunoblotting for Tel2, ATM, and mTOR in whole-cell lysates of the indicated cell lines using calibration with recombinant proteins as a standard. (B) Summary of the abundance of Tel2, ATM, and mTOR as determined in A. (C) Summary of Tel2-, Tti1-, and Tti2-associated proteins detected by mass spectrometry (see Supplemental Fig. 1). (D) Tel2 preferentially binds newly synthesized PIKKs. Immunoblots of Tel2-associated proteins in HeLa S3 cells treated with CHX (100 μ g/mL) as indicated. Tel2 was isolated by Flag-HA tandem affinity purification, and the associated proteins were detected by immunoblotting as indicated. (E) Tel2 does not bind ATM phosphorylated on S1981. HeLa S3 cells expressing Flag-[HA]2-Tel2 were γ -irradiated (20 Gy) and lysed after 1 h. ATM was detected by immunoblotting using MAT3 (total ATM) or phospho-ATM Ab (ATM S1981-P) after Flag/HA affinity purification of Tel2. (F) Effect of the geldanamycin derivative 17-AAG (Gel) on Tel2–PIKK interactions. HeLa S3 cells were treated as in D, except that 0.5 μ M 17-AAG was used to inhibit Hsp90 for the indicated times.

with Tti1 and Tti2, and revealed the presence of Pontin and Reptin in all three complexes. Pontin and Reptin (also known as Tip49A/B and RUVBL1/2) have been implicated in the function of a wide variety of nuclear protein complexes (Jha and Dutta 2009; Huen et al. 2010), and were shown recently to contribute to PIKK expression by affecting mRNA levels (Izumi et al. 2010). In addition, the Tti2 complex contained Hsp90 as well as PIH1D1 and RPAP3, which have been reported to associate with Hsp90, Pontin, and Reptin (Jeronimo et al. 2007; Te et al. 2007; Boulon et al. 2008; Gano and Simon 2010). The Tel2 and Tti1 complexes also showed evidence of an interaction with these proteins, and all three complexes contained Hsp70. These associations with molecular chaperones raised the possibility that the Tel2 complex plays a role in Hsp90-dependent maturation of PIKK complexes.

Tel2 preferentially binds newly synthesized ATM, ATR, mTOR, and DNA-PKcs

To determine whether Tel2 acts early in PIKK maturation, Tel2 complexes were isolated from HeLa cells treated with cycloheximide (CHX) to block translation. As expected, ATM, mTOR, ATR, and DNA-PKcs were recovered in the Tel2 IPs from control cells (Fig. 1D). However, this interaction was rapidly lost upon inhibition of translation. After 30 min in the presence of CHX, the recovery of ATM, mTOR, and DNA-PKcs was strongly diminished, and the association of Tel2 with ATR was clearly affected after protein synthesis was blocked for 60 min. The interaction of Tel2 with the PIKKs diminished despite the fact that the overall levels of neither Tel2 nor the PIKKs were affected by the short-term treatment with CHX (Fig. 1D). Furthermore, the effect was specific to the Tel2–PIKK interaction, as the binding of Tel2 to non-PIKK-interacting partners—including Tti1, Tti2, and Reptin—were unaffected (Fig. 1D). These data indicate that Tel2 interacts with these PIKKs within 1 h of their synthesis, but not beyond that time window. Consistent with this conclusion, we found that, when Tel2 complexes are isolated from irradiated cells, the phosphorylated form of ATM was not recovered (Fig. 1E). This result confirms that Tel2 does not associate efficiently with the activated and therefore mature form of ATM.

Inhibition of Hsp90 affects binding of Tel2 to ATM, ATR, mTOR, and DNA-PKcs

The finding that Tel2 interacts preferentially with nascent PIKKs and the recovery of several chaperones in the Tel2 complex raised the possibility that Tel2 functions in chaperone-mediated PIKK maturation. We therefore tested whether the Tel2–PIKK interaction is affected by inhibition of Hsp90 with the geldanamycin derivative 17-AAG. Tel2 complexes were isolated from HeLa cells that were treated with 17-AAG for 1 or 2 h, and the recovery of the PIKKs was evaluated (Fig. 1F). Short-term inhibition of Hsp90 did not affect the overall levels of these PIKKs or/and Tel2 (Fig. 1F). Whereas the interaction between Tel2 and Tti1, Tti2, and Reptin was not affected, the

binding of ATM, mTOR, ATR, and DNA-PKcs was diminished by Hsp90 inhibition. Consistent with this finding, our previous data indicated that prolonged (16–24 h) treatment with 17-AAG substantially diminished the levels of ATM and DNA-PKcs and had a minor effect on mTOR (Takai et al. 2007), and an inhibitory effect of geldanamycin on mTOR activation has been reported (Ohji et al. 2006).

Tel2 is required for the assembly of TORC1 and TORC2

To further dissect the effect of Tel2 on PIKK maturation, we used *in vivo* labeling to examine the formation of TORC2 by newly synthesized mTOR and Rictor (Fig. 2A). Consistent with previous data, at 60 h after deletion of Tel2 from Tel2^{F/-} MEFs, the level of mTOR was slightly diminished (Fig. 2B). Part of the remaining mTOR, presumably synthesized prior to complete Tel2 depletion, was associated with Rictor (Fig. 2C). In order to determine whether Tel2 affected the association between newly synthesized mTOR and Rictor, a protocol was developed that combined Tel2 deletion with labeling of newly synthesized proteins with ³⁵S-labeled methionine and cysteine. The abundance of ³⁵S-labeled mTOR in IPs of mTOR or Rictor was then quantified by autoradiography in three independent experiments. Consistent with our previous analysis, the absence of Tel2 did not strongly affect the synthesis rate of mTOR, resulting in approximately the same recovery of ³⁵S-labeled mTOR in mTOR IPs from cells with and without Tel2 (Fig. 2C). The recovery of mTOR in the Rictor IP from Tel2-proficient control cells showed that the protocol reliably detected newly synthesized mTOR in association with Rictor (Fig. 2D). Importantly, the recovery of newly synthesized mTOR in the Rictor IPs was strongly reduced when Tel2 was absent (Fig. 2D). Similarly, inhibition of Hsp90 with 17-AAG also reduced the association of newly synthesized mTOR with Rictor.

We next examined the effect of Tel2 on the formation of the TORC1 complex, consisting of mTOR, Raptor, and GβL. Because of the paucity of antibodies to the mouse TORC1 components, these experiments employed Tel2^{F/-} MEFs expressing Flag-tagged versions of Raptor and GβL. At the early time point examined, deletion of Tel2 from these MEFs had only a minor effect on the steady-state level of mTOR (Fig. 2E), the association of mTOR with Raptor (Fig. 2F), and the synthesis rates of mTOR (Fig. 2F) and Raptor (Fig. 2G). However, absence of Tel2 strongly diminished the association of newly synthesized mTOR with Raptor (Fig. 2G). A very similar result was observed with GβL, which also failed to associate efficiently with newly synthesized mTOR when Tel2 was absent (Fig. 2H–J). The incorporation of newly synthesized mTOR into the TORC1 complex was affected by 17-AAG (Fig. 2E–J), but the effect was much less pronounced than for the TORC2 complex.

We also compared the effects of Tel2 deletion or Hsp90 inhibition with those of rapamycin, which, together with FKBP12, binds to mTOR and weakens the mTOR–Raptor

Takai et al.

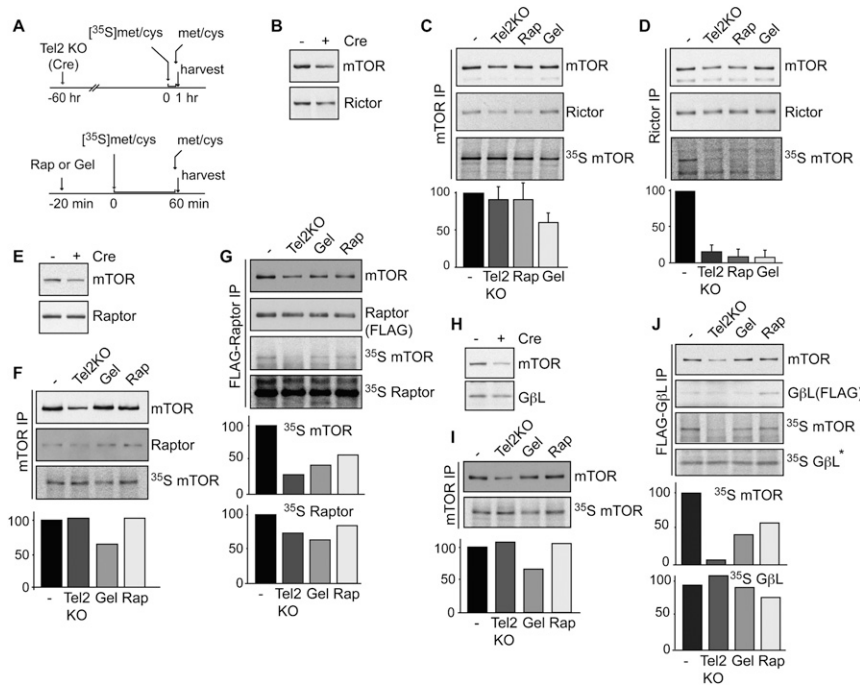


Figure 2. Tel2 deletion affects formation of TORC1 and TORC2. (A) Schematic of the in vivo labeling experiments. (Top) Experiments evaluating the effect of Tel2 deletion. Tel2^{F/-} MEFs were treated for 6 h with 0.5 μ M 4-hydroxytamoxifen to induce Cre and delete Tel2 (Tel2 KO) or were left untreated. Sixty hours later, the cells were labeled with ³⁵[S]-methionine and ³⁵[S]-cysteine for 1 h and washed with regular media before harvesting. (Bottom) Experiments evaluating the effect of 17-AAG (Gel) and rapamycin (Rap). Tel2-proficient MEFs were pretreated for 20 min with 0.1 μ M rapamycin or 0.5 μ M Hsp90 inhibitor 17-AAG and then labeled for 1 h as described above in the presence of the drugs. (B) Immunoblots for mTOR and Rictor in cells with and without Tel2. (C, top panels) Immunoblots to detect total mTOR and Rictor, and autoradiography to detect ³⁵S-mTOR in mTOR IPs from cells treated as indicated. The bar graph at the bottom shows the relative ³⁵S-mTOR signal in the lanes above; values represent averages, and the error bars represent the standard deviations derived from three independent

experiments. (D) As in C, but using Rictor antibodies for the IPs. (E) Immunoblots for mTOR and Flag-Raptor in cells with and without Tel2. (F, top panels) Immunoblots to detect total mTOR and Raptor, and autoradiography to detect ³⁵S-mTOR in mTOR IPs from cells treated as indicated. (G) As in F, but using Flag IP for Raptor. The top two panels are immunoblots for mTOR and Raptor, and the bottom panels represent detection of ³⁵S-labeled proteins. Bar graphs show the relative recovery of ³⁵S-labeled mTOR and Raptor in the Raptor (Flag) IPs, determined based on the lanes shown above. (H) Immunoblots for mTOR and Flag-GβL in cells with and without Tel2. (I) Immunoblots to detect total mTOR, and autoradiography to detect ³⁵S-mTOR in mTOR IPs from cells treated as indicated. The bar graph at the bottom shows the relative ³⁵S-mTOR signal in the lanes above. (J) As in G, but using Flag IP for GβL. The top two panels are immunoblots for mTOR and GβL, and the bottom panels represent detection of ³⁵S-labeled proteins. The ³⁵S GβL signal overlaps with a weak nonspecific signal (asterisk). Bar graphs showing the relative recovery of ³⁵S-labeled mTOR and GβL in the GβL (Flag) IPs, determined based on the lanes shown above.

association (Kim et al. 2002). Although rapamycin cannot bind to the preformed TORC2 complex, prolonged rapamycin treatment has been shown to decrease steady-state TORC2 levels by inhibiting the assembly of newly synthesized mTOR into TORC2 complexes (Sarbasov et al. 2006). Figure 2, E–J, shows that the inhibition of TORC1 assembly by rapamycin was partial and comparable with what is observed with 17-AAG treatment. In contrast, assembly of newly synthesized mTOR into TORC2 complexes was strongly inhibited by rapamycin, and again this paralleled the pronounced effects of Tel2 deletion and 17-AAG treatment (Fig. 2D).

Collectively, these data indicate that Tel2 is important for the incorporation of newly synthesized mTOR into the TORC1 and TORC2 complexes. A requirement for the human Tel2/Tti1/Tti2 complex in the formation of TORC1 and TORC2 was inferred by Kaizuka et al. (2010).

Tel2 is required for the association of ATR with ATRIP

To determine whether these results applied to other PIKKs, we focused on the ATR kinase because it has a well-described interacting partner, ATRIP, that is required for ATR signaling (Zou and Elledge 2003). To test

how Tel2 affects the formation of the ATR–ATRIP complex, Tel2^{F/-} MEFs were infected with Flag-tagged mouse ATRIP to allow for efficient ATRIP immunoprecipitation. Using these cells, the Tel2-dependent association of newly synthesized ATR and ATRIP was monitored by coimmunoprecipitation of in vivo labeled proteins, as described above (Fig. 2A). Tel2 was deleted, and the level and association of ATR and ATRIP were monitored after 60 h (Fig. 3A). Although the ATR level eventually diminished after Tel2 deletion, ATR was still present at 60 h, and this residual ATR formed a complex with ATRIP (Fig. 3A,B). Furthermore, the rates of synthesis of ATR and ATRIP were not strongly affected by the absence of Tel2, resulting in only a minor reduction in the recovery of ³⁵S-labeled ATR and ATRIP in IPs for ATR and ATRIP, respectively (Fig. 3B,C). However, the recovery of newly synthesized ATR in the ATRIP IPs was strongly diminished in cells lacking Tel2 (Fig. 3C), indicating impaired formation of the mature ATR–ATRIP complex. The association of newly synthesized ATR with ATRIP was also diminished by inhibition of Hsp90 with 17-AAG (Fig. 3C). Thus, Tel2 and Hsp90 affect the formation of the ATR–ATRIP complex and the TORC1 and TORC2 complexes in a similar fashion.

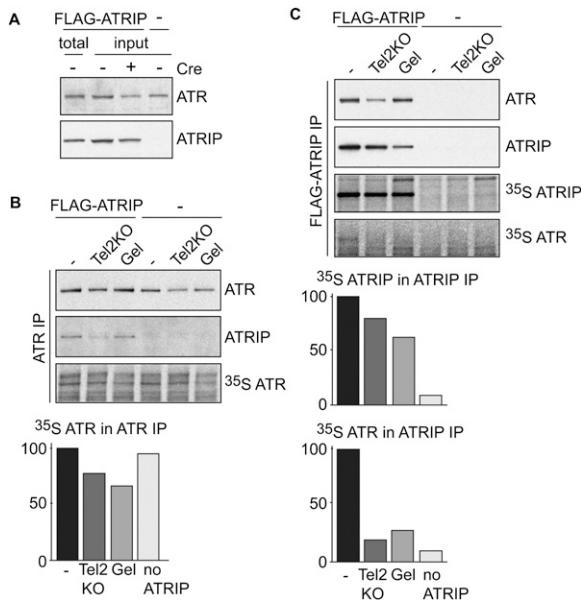


Figure 3. ATR and ATRIP complex formation depends on Tel2 and Hsp90 activity. (A) Immunoblots for ATR and Flag-ATRIP in cells with and without Tel2. (Last lane) Cells lacking Flag-ATRIP. (B, top panels) Immunoblots to detect total ATR and Flag-ATRIP, and autoradiography to detect ^{35}S -ATR in ATR IPs from cells treated as indicated. Cells were treated as in Figure 2A. The bar graph at the bottom shows the relative ^{35}S -ATR signal in the lanes above. (C) As in B, but using Flag IP for ATRIP. The top two panels are immunoblots for ATR and Flag-ATRIP, and the bottom panels represent detection of ^{35}S -labeled proteins. The bar graphs show the relative recovery of ^{35}S -labeled ATRIP and ATR in the ATRIP (Flag) IPs, determined based on the lanes shown above.

Tel2 domain organization, crystallization, and structure determination

The Tel2 structure was determined using budding yeast Tel2 (residues 1–688) that contained an internal deletion (residues 387–427) (Fig. 4A). The deleted region is highly susceptible to proteolytic digestion, is poorly conserved, and consists predominantly of polar and charged residues (Supplemental Fig. 2). Proteolysis of this region resulted in the chromatographic separation of the flanking N-terminal and C-terminal structured portions, suggesting that it is a flexible linker that links two independently folded structural domains. Crystals of the internally truncated budding yeast Tel2 (hereafter, scTel2) formed in space group $P2_1$ and contained four molecules in the asymmetric unit. The structure was determined by the single-wavelength anomalous dispersion (SAD) method using selenomethionine-substituted scTel2, and was refined at 3.1 Å resolution to a free R -factor of 23.9% (Supplemental Table 1).

scTel2 structure

As predicted from sequence analyses (Anderson et al. 2008), Tel2 is a helical repeat protein in which pairs of interacting helices pack side by side to form a superhelical assembly, or α -solenoid (Andrade et al. 2001b). The scTel2 helical repeats fold into two distinct solenoids that es-

entially correspond to the two structural domains identified by limited proteolysis.

The N-terminal solenoid (hereafter, NTD) consists of residues 1–354 and contains 21 α -helices ($\alpha 1$ – $\alpha 21$) (Fig. 4B). The chain then folds back, and residues 355–386 extend toward the middle of the NTD, packing with NTD residues along the way. This extended segment leads to the C-terminal solenoid (hereafter, CTD; residues 428–688), which has 11 α -helices ($\alpha 22$ – $\alpha 32$). The CTD projects away from the middle of the NTD, in a nearly perpendicular orientation (Fig. 4B). In the crystals, the NTD and CTD domains pack loosely through a handful of residues that are not conserved. Because proteolysis of the NTD–CTD linker results in the dissociation of the two domains on gel filtration chromatography, we presume that this NTD–CTD association is either weak or absent in the full-length protein.

The helical repeats of the NTD solenoid are rather irregular, exhibiting a wide range of intra- and interrepeat packing angles, with several extra helices in between repeats (Supplemental Fig. 2). A structural homology search with the program DaliLite (Holm et al. 2008) identified significant structural relatives only for the last

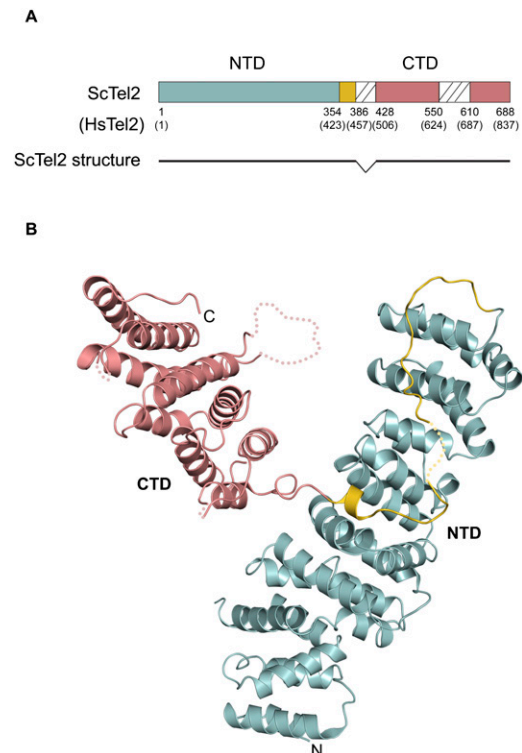


Figure 4. Overall structure of scTel2. (A) Schematic representation of Tel2. The domains discussed in the text, with their residue numbers for scTel2 and human Tel2 (HsTel2, in parentheses), are indicated, with the NTD colored cyan, the CTD colored pink, and the extended segment after the last NTD helical repeat in yellow. The two protease-sensitive flexible loops are marked with hatched lines. The crystallized scTel2 construct is shown as a line. (B) Overall view of scTel2, colored as in A. Dotted lines indicate disordered regions.

Takai et al.

three repeats ($\alpha 15$ – $\alpha 21$), with root-mean-square deviations (RMSDs) of 2.9–3.2 Å over the C α positions of ~110 residues (Z scores of 8.1–8.7) (Supplemental Table 2). The closest structural homologs are the VHS domain of STAM1 and a portion of importin β , which belong to the HEAT repeat family of superhelical proteins, and in particular to the IMB subfamily (Andrade et al. 2001b). Compared with the prototypical HEAT repeats found in the protein phosphate 2A 65-kDa constant regulatory subunit (Pr65A), the IMB subfamily is more degenerate, lacking, for example, the characteristic Pro-induced bends on the outer helices (the repeat helix on the convex surface of the solenoid is referred to as the outer helix, while that on the concave surface is referred to as the inner helix), as well as the common interrepeat salt bridges (Andrade et al. 2001b). One property of the last three NTD repeats that matches well to the VHS domain is a pronounced kink in the middle repeat that diverges from a regular repeat structure. In the STAM1-VHS domain, this kink forms part of the ubiquitin-binding site (Ren and Hurley 2010). The corresponding region of Tel2 is involved in packing with the extended polypeptide segment that follows the last NTD repeat.

The CTD solenoid contains a more regular arrangement of four repeats ($\alpha 24$ – $\alpha 31$), and a terminal helix ($\alpha 32$) that caps the last repeat. A DaliLite search identified several structures with substantial structural homology across the entire length of the CTD (Z scores of ~11) (Supplemental Table 2). These include the prototypical HEAT repeat protein Pr65A (3.5 Å RMSD over 164 residues; $Z = 10.6$) and the TOG domain of a family of microtubule-binding proteins (3.0 Å RMSD over 164 residues; $Z = 11.3$). Several conformational features characteristic of the Pr65A HEAT repeats are variably present in the Tel2 CTD. These include a proline-induced kink in the outermost repeat helix (at Pro625 of repeat 4), as well as an interrepeat Arg/Lys–Asp/Glu salt bridge (Lys644–Glu681 between repeat 4 and $\alpha 32$). One area of divergence from a canonical HEAT repeat arrangement is the packing angle between the second and third repeats, which has a negative twist (approximately -30° angle between helical axes) compared with typically small twists in canonical repeats. This results in a surface crevice centered on the second helix of repeat 3 ($\alpha 29$), flanked by the second helices of repeats 2 and 4 ($\alpha 26$ and $\alpha 31$). Interestingly, a very similar interrepeat packing feature with a large negative twist and surface crevice occurs in Pr65A, and this similarity likely contributes the high score of the structural alignment between the two proteins (Supplemental Fig. 3). In Pr65A, this crevice is involved in binding the catalytic subunit of protein phosphatase 2A, and, as discussed below, sequence conservation suggests that the analogous Tel2 CTD region may be involved in protein–protein interactions as well.

Evolutionarily conserved elements of the scTel2 structure

As a first step in identifying the functionally important regions of the Tel2 structure, we mapped orthologous

sequence conservation onto the structure. Because Tel2 orthologs exhibit overall low sequence conservation, we used the structure of scTel2 to guide a multiple sequence alignment using the Indonesia program (D Madsen, P Johansson, N Johansson, S Arent, MR Harris, and GJ Kleywegt, in prep.). In this alignment, the NTD displays less conservation than the CTD, with 12.2% and 19.8% identity, respectively, between the human and yeast sequences (Fig. 5A; Supplemental Fig. 2). The overall sequence similarity is not uniformly distributed, with conserved residues clustering near the end of the NTD (residues 328–358) and in the middle portion of the CTD (residues 499–626), excluding its disordered region (550–610).

When the conservation is mapped onto the solvent-accessible surface of scTel2, the conserved NTD residues cluster in a single surface patch formed by the last two helices of the solenoid ($\alpha 20$ and $\alpha 21$) (Fig. 5A,B; Supplemental Fig. 2). The best conserved of these residues are Leu333, Arg341, and Met345. They are mostly solvent-exposed, although they still have structural roles. Their side chains make van der Waals contacts to each other, while Arg341 also makes a hydrogen bond to the backbone carbonyl group of Ser335, and Met345 also packs with Tyr358 (Fig. 5B). The conservation of these residues, while attributed in part to their structural roles, indicates that this region plays an important role in Tel2 function, especially in the background of much lower conservation in the rest of the NTD, including its buried structural residues (Fig. 5A; Supplemental Fig. 2).

On the CTD, the conservation maps to a wide surface band that encircles the middle portion of the domain (helices $\alpha 27$ – $\alpha 30$) (Fig. 5A; Supplemental Fig. 3). This band of surface conservation is significantly larger and more diffuse than that of the NTD, encompassing the second helix of repeat 2 ($\alpha 27$), the entire repeat 3 ($\alpha 28$ – $\alpha 29$), and the first helix of repeat 4 ($\alpha 30$). Within this broad band, the tip of repeat 3 ($\alpha 28$ – $\alpha 29$ loop) stands out with a cluster of five highly conserved residues (Phe526, Ser531, Leu532, Gln534, and Arg535) (Supplemental Fig. 3A). Here, Ser531 and Leu532 are mostly solvent-exposed, with few apparent structure-stabilizing roles, while the Arg535 side chain hydrogen bonds to a pair of backbone carbonyl groups of the $\alpha 28$ – $\alpha 29$ loop, stabilizing the local conformation of this loop. Phe526 and Gln534 have more extensive structural roles, stabilizing interrepeat packing through van der Waals contacts and hydrogen bond networks, respectively (Supplemental Fig. 3A). The tip of repeat 3 is part of the surface crevice formed by the noncanonical packing of the second and third repeats discussed above (Supplemental Fig. 3B). As observed with Pr65A, protein–protein interaction sites on helical repeat proteins are often associated with a divergence from a canonical repeat structure, and these regions tend to exhibit higher sequence conservation due to intermolecular contacts and the requirement to maintain the precise structural framework that supports these contacts. Thus, the tip of repeat 3 may have a function in protein–protein interactions, although, given the extent of conservation throughout the surface band of

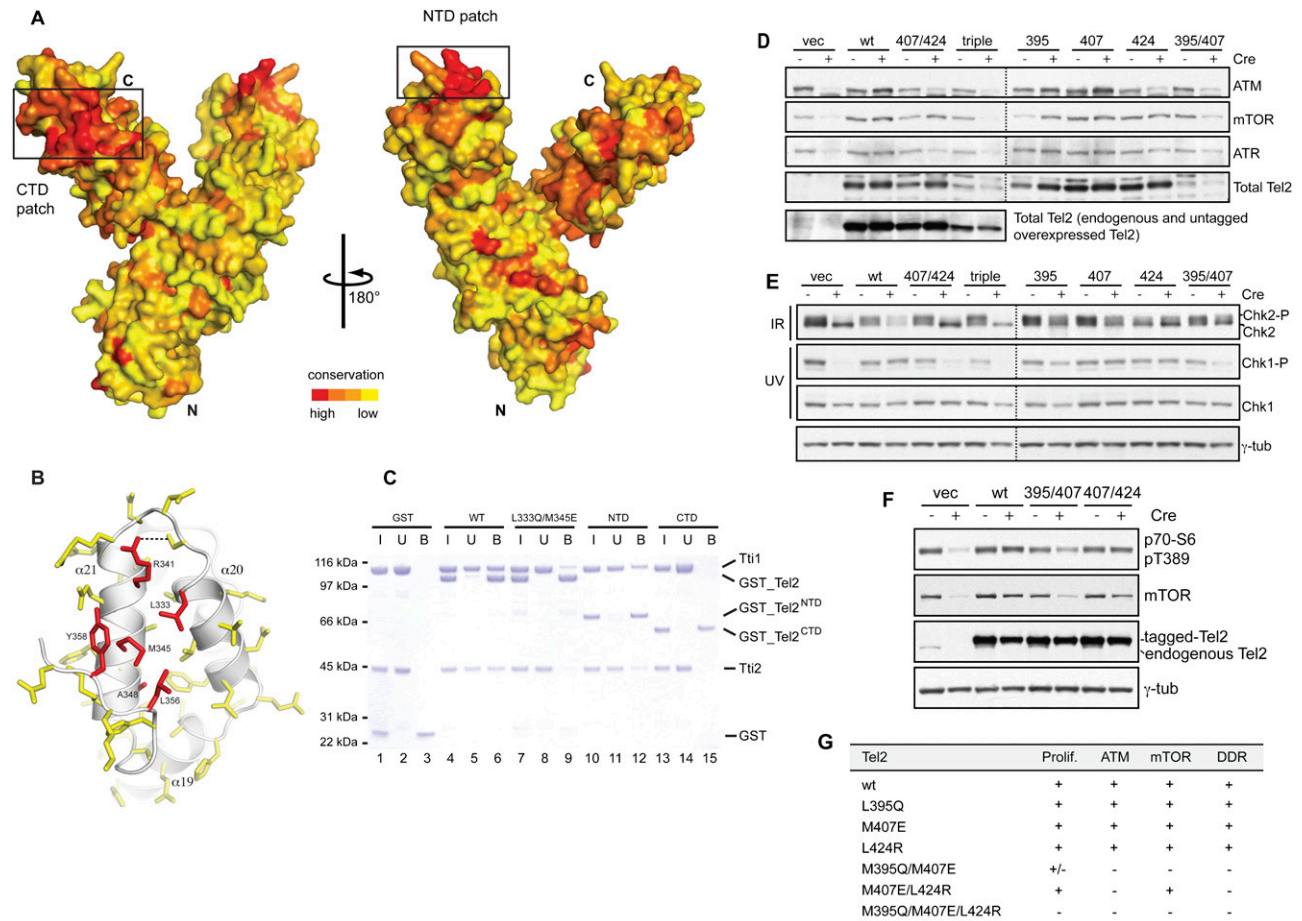


Figure 5. Direct binding of the conserved NTD patch to Tti1-Tti2 important for Tel2 function. (A) Molecular surface representation of scTel2 colored according to conservation among Tel2 orthologs [see Supplemental Fig. 2 for sequence alignment]. (B) Close-up view of the conserved NTD patch shown in A. The highly conserved residues are colored red. (C) Binding of GST-scTel2 to Tti1-Tti2 complex. In vitro pull-down assay was carried out with purified recombinant proteins. Input (I), unbound (U), and bound (B) fractions were analyzed using a Coomassie-stained SDS-PAGE gel. The NTD but not CTD of scTel2 binds to the Tti1-Tti2 complex (cf. lanes 12 and 15). The L333Q/M345E mutant binds substantially lower amounts of the Tti1-Tti2 complex (cf. lanes 6 and 9). (D) Effect of Tel2 mutations on the stability of ATM, mTOR, and ATR. The indicated alleles of Tel2 were introduced into Tel2^{F/-} MEFs, and the endogenous Tel2 was deleted with 4-hydroxytamoxifen induction of Cre. At 120 h post-Cre, whole-cell lysates were analyzed by immunoblotting for the indicated proteins. (E) Effect of Tel2 mutations on the DNA damage response. The cells described in D were treated with IR (2 Gy) or UV (25 J/m²), and were processed for immunoblotting after 30 min and 1 h, respectively. The DNA damage response was monitored based on phosphorylation of Chk2 (top) and Chk1 (S345-P) (bottom). (F) Effect of Tel2 mutations on mTOR signaling after serum stimulation. (G) Summary of the phenotypes associated with Tel2 mutations. Levels of mTOR and ATM were determined as in D. The DNA damage response (DDR) was determined as in E. Proliferation (Prolif.) of cells treated with Cre was measured over 9 d.

the CTD, this putative protein-binding site may involve a substantially large area.

The protease-sensitive NTD-CTD linker that was deleted from the crystallized scTel2 exhibits overall low sequence conservation, but a cluster of acidic residues (residues 418–427 in scTel2) present in most Tel2 orthologs may be important for Tel2 function. In addition, the length of the linker and the resulting spatial separation of the NTD and the CTD may be important for Tel2 function as well.

The scTel2 NTD binds directly to Tti1-Tti2 complex

To investigate whether the conserved regions of the scTel2 structure are involved in protein-protein interactions, we first sought to identify components of the Tel2

complex that may interact directly with Tel2. We chose to test the Tti1-Tti2 complex, as it is present in Tel2 complexes isolated from both fission yeast and mammalian cells (Fig. 1C; Hayashi et al. 2007). Figure 5C shows that the insect cell-expressed and purified Tti1-Tti2 complex binds to GST-scTel2 but not GST when an equimolar mixture of the proteins is isolated using glutathione beads. We then tested the individual NTD and CTD domains of scTel2 and found that the Tti1-Tti2 complex can bind to the GST-NTD but not the GST-CTD fusion proteins. Although we cannot rule out a contribution by the CTD, these data indicate that the major Tti1-Tti2-binding site resides within the NTD.

We next addressed whether the conserved surface patch of the NTD is involved in this interaction. For this,

Takai et al.

we made the Leu333-to-Gln and Met345-to-Glu (L333Q/M345E) double mutation in the context of full-length scTel2. This double mutation does not noticeably affect the overall structure and stability of scTel2, as the insect cell-expressed mutant protein has overexpression levels, solubility, and a gel filtration chromatography profile comparable with those of wild-type scTel2 (data not shown). Yet, in the GST pull-down assay, the GST-Tel2^{L333Q/M345E} double mutant binds substantially lower amounts of the Tti1–Tti2 complex (Fig. 5C, cf. “bound” lanes 6 and 9, and “unbound” lanes 5 and 8). This indicates that the last NTD helical repeat is involved in Tti1–Tti2 binding, providing one explanation for its relatively high level of conservation.

The Tti1–Tti2-binding site of Tel2 is important for its in vivo function

To examine the role of the Tti1–Tti2-binding site at the conserved NTD patch, we tested mouse Tel2 point mutants for their ability to complement phenotypes associated with Tel2 deletion from Tel2^{F/-} MEFs (Fig. 5D–G). For this, we mutated mouse Tel2 at Leu395 (corresponding to yeast Leu333), Met407 (corresponding to yeast Met345), and Leu424 (corresponding to yeast Leu356, immediately after the end of the last NTD repeat), alone or in combinations.

As shown previously, deletion of Tel2 from MEFs results in a proliferation defect; diminished ATM, mTOR, and ATR protein levels; a deficiency in the response to UV- or IR-induced DNA damage; and diminished mTOR signaling (Takai et al. 2007). Each of these phenotypes was rescued when the Tel2-deficient cells were complemented with the wild-type Tel2 (Fig. 5D–G). When introduced as single-point mutants, the L395Q, M407E, and L424R alleles were indistinguishable from wild type, rescuing these phenotypes. We note, however, that the exogenous Tel2 in these experiments is expressed at substantially higher levels than the endogenous protein (Fig. 5D,F), and it is possible that these higher levels would compensate for a weaker association of mutant Tel2 with Tti1–Tti2. Indeed, when we tested the L395Q/M407E/L424R triple mutant, we found it was defective in rescuing any of these phenotypes (Fig. 5D–G). Although this mutant was expressed at lower levels compared with the single mutant or wild-type Tel2, its levels were still much higher than the endogenous Tel2 (Fig. 5D).

The L395Q/M407E double mutant had an intermediate phenotype, failing to fully restore levels of the PIKKs, checkpoint function, and mTOR signaling, and only partially restoring the proliferation defect. Interestingly, the M407E/L424R double mutant exhibited a mixed phenotype. It failed to fully restore ATM and ATR levels, and consequently had a checkpoint defect (Fig. 5D,E). Both the phosphorylation of Chk2 in response to IR, a readout for ATM activity, and the phosphorylation of Chk1 after UV, reporting on ATR activity, were strongly diminished (Fig. 5E). However, this double mutant largely restored mTOR levels and signaling and rescued the growth defect (Fig. 5F,G). Thus, the M407E/L424R mutant

of Tel2 appears to be a dissociation-of-function mutant that is proficient with regard to mTOR but impaired with regard to ATM and ATR (Fig. 5D,E). Such dissociation-of-function mutants were previously invoked to explain the pleiomorphic phenotypes of the various point mutations in the Tel2/Clk-2 genes of worms and yeast (Takai et al. 2007). One possible explanation for this may be that the conformational maturation of ATM and ATR is more critically dependent on the full function of the Tel2 complex compared with that of mTOR.

Discussion

Taken together, our data suggest that the PIKKs depend on Hsp90 and Tel2–Tti1–Tti2 for their maturation. In vivo labeling showed that the PIKKs bind to Tel2 soon after their synthesis in a manner that is dependent on Hsp90 function. The formation of three PIKK complexes—TORC1, TORC2, and the ATR–ATRIP complex—was impaired when Tel2 was absent or when Hsp90 was inhibited. Once mature, the PIKK complexes were no longer associated with Tel2. Tel2 mutants defective in Tti1–Tti2 binding were impaired in their ability to rescue the growth and checkpoint defects associated with deletion of Tel2 from MEFs, indicating that the function of Tel2 in the mTOR, ATM, and ATR pathways also requires the Tti1–Tti2 complex. The Tel2 complex also contains Hsp90, Hsp70, and Hsp40. It is likely that Tel2 and Hsp90 act in concert to mediate the maturation of mTOR and ATR, allowing these kinases to form functional complexes with their specific interacting partners. We propose that Tel2–Tti1–Tti2 and Hsp90 similarly promote the maturation of the other PIKKs.

The nature of the maturation reaction Hsp90 catalyzes is not well understood, although it is thought to occur after the initial folding process. In general, Hsp90 clients are proteins that are not yet fully active, due to either the absence of a binding partner/substrate required for activation or the lack of post-translational modification. With the nuclear hormone receptors, which are delivered to Hsp90 through the action of Hsp70, the Hsp90 complex is required to keep a large hydrophobic cavity in the ligand-binding domain (LBD) in a conformation that can bind to the hormone (Young et al. 2001; Wandinger et al. 2008). With conventional Ser/Thr kinase clients, an Hsp90 complex that contains the kinase domain-specific Cdc37 cochaperone is required for the production of active forms of the kinases, although the manifestations of Hsp90 action differ with different kinases (Young et al. 2001; Wandinger et al. 2008). With Cdk4, Hsp90 is required for the eventual assembly with the requisite Cyclin D subunit, whereas, with monomeric kinases such as Raf and Akt, it may be required prior to a regulatory phosphorylation that causes a conformational change and activates the kinase. A distinct category of clients involves certain destabilized proteins such as the oncoprotein v-src, whose mutation results in reduced thermodynamic stability compared with the nonclient c-src (Wandinger et al. 2008).

Our findings that the Tel2–Tti1–Tti2 complex is required for the assembly of mTOR and ATR with their

respective partners are reminiscent of the action of Cdc37 in the activation of Ser/Thr kinases. Like Cdc37, the Tel2–Tti1–Tti2 complex may not only help recruit PIKKs to Hsp90 complexes, but it also may affect the Hsp90 ATPase cycle in a manner that is optimal for this specific class of substrates (Gray et al. 2008). However, while Cdc37 specifically associates with the catalytic domain of Ser/Thr kinases, several studies have shown that it is the PIKK helical repeat regions, often involving multiple discontinuous segments, that the Tel2–Tti1–Tti2 complex associates with (Takai et al. 2007; Anderson et al. 2008). This suggests that the action of Tel2–Tti1–Tti2 involves, at least in part, a property of the PIKK helical repeat regions.

One unique property of helical repeat proteins may be their folding process. Unlike globular proteins, where a unit of up to 250 amino acids folds cooperatively (Garel 1992), the folding of very large solenoid proteins may be nucleated at multiple positions and proceed sequentially along the primary sequence (Andrade et al. 2001a). Nevertheless, as in globular proteins, solenoid proteins may also have interactions between helical repeats that are distant from each other in the primary sequence, and this feature may be common in PIKKs. Electron microscopy (EM) reconstructions of ATM and mTOR (Llorca et al. 2003; Adami et al. 2007), and the 6.6 Å structure of DNA-PKcs (Sibanda et al. 2009), exhibit large globular-like regions that would require a number of interactions between nonsequential segments involving not only the helical repeats, but the C-terminal PI3K-like kinase domain as well. In fact, crystal structures of PI3Ks show interactions between the kinase domain and helical repeat segments (Amzel et al. 2008). Since such interactions are likely to involve, at least in part, hydrophobic residues, the Hsp90–Tel2 chaperone system may prevent the aggregation of locally folded helical segments with exposed hydrophobic regions until all of the interacting segments—and in particular the C-terminal kinase domain—are synthesized, have completed their local folding, and are able to make intramolecular interactions. In this respect, the requirement of Hsp90 for the association of mTOR and ATR with their binding partners may reflect an indirect role where the PIKK has to complete its overall folding before it can bind to its partner. Additionally, the Hsp90–Tel2–Tti1–Tti2 complex may also help sequester exposed hydrophobic regions on the PIKK helical repeats to which Raptor and ATRIP bind (Kim et al. 2002; Ball et al. 2005).

Materials and methods

Cell culture

Tel2-inducible knockout mice were generated as described (Takai et al. 2007). Tel2^{FLOX/+} (Tel2^{F/+}) mice were crossed with R26Cre-ER^T transgenic mice [B6;129-Gt(ROSA)26Sor^{tm1(cre/ERT)Nat1/J}, #004847; Jackson Laboratories] (Badea et al. 2003). Primary MEFs were isolated from 13.5-d embryos and maintained in DMEM supplemented with 15% fetal calf serum (FCS), 1 mM sodium pyruvate, 100 U of penicillin, and 0.1 μg of streptomycin per

milliliter; 0.2 mM L-glutamine; and 0.1 mM nonessential amino acids, and then immortalized by infection with retroviral SV40-LT. Transformed MEFs and HeLa S3 and HTC75 cells were cultured in the same media with 10% FCS without sodium pyruvate. HeLa S3 cells in suspension culture were maintained in Joklik's medium (M0518, Sigma) with 10% FBS. To induce Cre-recombinase-mediated Tel2 gene deletion, MEFs were incubated for 5 h with 0.5 μM 4-OHT (Sigma).

Immunoblotting and antibodies

Cells were harvested by trypsinization, lysed in 2× Laemmli buffer (100 mM Tris-HCl at pH 6.8, 200 mM DTT, 4% SDS [w/v], 20% glycerol, 0.05% bromophenol blue) at 1 × 10⁴ cells per microliter, denatured for 10 min at 80°C, sheared with an insulin syringe, and resolved on SDS/PAGE gels using the equivalent of 2 × 10⁵ cells per lane. After immunoblotting, the membranes were blocked in PBS/0.1% Tween-20 with 5% nonfat dry milk, and primary antibodies were incubated in PBS/0.1% Tween-20 with 0.1%–5% nonfat dry milk. Anti-mTel2 mouse polyclonal antibody and anti-hTel2C were described before (Takai et al. 2007). Anti-hTti1 and anti-hTti2 mouse polyclonal antibodies were produced using bacterial GST-tagged full-length hTti1 and hTti2 proteins after the removal of GST tag. The antisera were used without further purification. Additional antibodies were ATM and MAT3 (Sigma); phospho-ATM (Cell Signaling Technology); ATR and N-19 (Santa Cruz Biotechnology); DNA-PKcs and Ab-4 (Lab Vision); mTOR (Cell Signaling Technology); Chk1 (Santa Cruz Biotechnology); Chk1 pS345 (Cell Signaling Technology); Chk2 (BD Biosciences); γ-tubulin (GTU-88, Sigma); Reptin (TIP49b, BD Transduction Laboratories); Hsp90 (HSP90β, Abcam); Hsp70 (BD Biosciences); Hsp40 (HDJ2, Abcam); PIH1D1 (Abcam); and p70-S6K pT389 (Cell Signaling Technology).

Recombinant proteins

ATM and mTOR cDNA fragments coding amino acids 1690–2120 and 2000–2549, respectively, were amplified by PCR using human ATM and rat mTOR cDNAs as templates, cloned into pGEX-4T-2. These fragments contain the epitopes for the antibodies for ATM and mTOR used for quantitative immunoblotting. The recombinant GST fusion proteins were purified as described previously (Takai et al. 2007). N-terminally [His]6-tagged hTel2 cloned in pBacPac was purified as described (Takai et al. 2007). Proteins were resolved by SDS-PAGE and stained by SimplyBlue SafeStain (Invitrogen).

Proteomic analysis

Isolation of the human Tel2, Tti1, and Tti2 complex was performed by Flag-HA tandem affinity purification from 1 × 10⁹ HeLa S3 cells expressing N-terminal Flag-[HA]2-tagged hTel2, hTti1, and hTti2. HeLa S3 cells were collected, rinsed in cold PBS, and disrupted by homogenization in 1 mL of lysis buffer (40 mM HEPES at pH 7.5, 120 mM NaCl, 10% glycerol, 1 mM EDTA, 5 mM β-mercaptoethanol, 1 mM PMSF, 1× Complete protease inhibitor mix, 1× PhosSTOP phosphatase inhibitor mix [Roche]) on ice. The lysate was cleared by centrifugation at 16,000g for 15 min at 4°C. Sequential IPs were done with anti-Flag M2 beads and elution with 3× Flag peptide (Sigma), followed by anti-HA beads and elution with HA peptide (Roche). Eluted proteins were separated by SDS-PAGE (8%–16% gradient; Invitrogen), visualized by Colloidal Blue Staining Kit (Invitrogen), excised, and subjected to trypsin digestion. The resulting peptides were extracted and identified by MALDI-TOF mass spectrometry at the Rockefeller University Proteomics Resource Center.

Takai et al.

Metabolic labeling

Mouse ATRIP, Raptor, and GβL were amplified by PCR and cloned into a pBabe-NFlag retrovirus vector. 1.5×10^6 cells were plated per 10-cm dish 1 d prior to the labeling. Cells were rinsed with methionine and cysteine (met/cys)-free DMEM (#21013-024, GIBCO) three times and incubated with 4 mL of labeling medium (met/cys-free DMEM, 10% dialyzed FBS, 2 mM L-glutamine) containing 0.1 mCi/mL [³⁵S]-met/cys mix (EasyTag EXPRESS ³⁵S protein labeling mix, NEG772007MC, PerkinElmer) for 1 h at 37°C. The medium was replaced with normal culture medium (DMEM supplemented with 10% FCS, non-essential amino acids, and glutamine). The cells were rinsed with cold PBS twice and collected by scraping in 1 mL of lysis buffer (40 mM HEPES at pH 7.5, 120 mM NaCl, 10% glycerol, 1 mM EDTA, 5 mM β-mercaptoethanol, 1 mM PMSE, 0.3% CHAPS, 1× Complete protease inhibitor mix, 1× PhosSTOP phosphatase inhibitor mix [Roche]). For Flag-tagged Raptor IPs, cells were scraped in the same lysis buffer without CHAPS and disrupted by sonication. The lysate was cleared by centrifugation at 16,000g for 15 min at 4°C. IPs were performed with anti-mTOR (Cell Signaling Technology), anti-Rictor (Abcam), and anti-ATR (Santa Cruz Biotechnology) antibodies. Samples were nutated for at least 3 h at 4°C and then incubated with protein G Sepharose beads (GE Healthcare) for at least 1 h. Flag-tagged proteins were immunoprecipitated by anti-Flag M2 beads (Sigma). The beads were washed four times with lysis buffer without CHAPS. Precipitates were dissolved in 2× Laemmli buffer and separated by SDS-PAGE. The gels were immersed in Amplify (NAMP100V, Amersham), dried, and exposed to a PhosphorImager screen (GE Healthcare). The quantification of the signal incorporated into mTOR proteins was performed with the Storm imaging system and the ImageQuant software (GE Healthcare).

Assays for ATM, ATR, and mTOR signaling

The effect of Tel2 on PIKK signaling was determined as described previously (Takai et al. 2007). Briefly, 0.8×10^6 MEFs per 6-cm dish were plated 18–24 h before the experiments. Cells were exposed to 2 Gy of γ-rays or 20 J/m² UV light and cultured for 30 min or 1 h, respectively, at 37°C. For UV treatment, the culture was rinsed with D-PBS (containing 0.9 mM CaCl₂, 0.5 mM MgCl₂) once and irradiated without lid. For the mTOR signaling assay, 0.5×10^6 MEFs per 6-cm dish were plated and cultured for 18–24 h. For serum starvation and restimulation, cells were incubated in DMEM without supplements for 20 h and then supplied with complete media for 30 min. Cell lysates were prepared by adding 200 μL of 2× Laemmli buffer to the dishes. Twenty microliters of lysates was applied to 8% Tris-glycine SDS-PAGE.

Protein expression and purification

Saccharomyces cerevisiae Tel2 (GenBank ID: NP_011613) was amplified from genomic DNA (Novagen). All point mutants and internal deletion constructs of Tel2 were generated by overlap PCR. GST-tagged *S. cerevisiae* Tel2 proteins were expressed in baculovirus-infected insect cells. Tel2^{NTD} (residues 1–386) and Tel2^{CTD} (residues 387–688) were expressed as GST fusion proteins in *Escherichia coli*. The cells are lysed at 4°C in 20 mM Tris-HCl, 500 mM NaCl, 5% glycerol, 10 mM DTT, 1 mM PMSE, and 1 μg/mL each aprotinin, leupeptin, and pepstatin (pH 8.0). They were first purified by glutathione affinity chromatography followed by TEV cleavage of the GST tag, then by anion exchange and gel filtration chromatography. The *S. cerevisiae*

Tti1 (GenBank ID: NP_012892) and Tti2 (GenBank ID: NP_012670) were amplified from *S. cerevisiae* genomic DNA. His-tagged Tti1 and GST-tagged Tti2 were coexpressed in insect cells and purified with a similar protocol as Tel2.

Crystallization and structure determination

Crystallization trials were carried out with scTel2 expressed in insect cells using a baculovirus vector, as human Tel2 had very limited solubility and was prone to aggregation (data not shown). Because full-length yeast Tel2 failed to produce crystals in extensive trials, limited proteolysis was used to probe the domain organization of the protein. These experiments revealed the presence of two regions that are highly susceptible to proteolysis. Digestion of the first region (residues 387–427) resulted in the chromatographic separation of the flanking N-terminal and C-terminal structured portions. This suggested that the first protease-sensitive region is a flexible linker that links two independently folded structural domains that either are not interacting or are interacting weakly. In contrast, digestion of the second region (residues 550–610) did not result in the dissociation of the flanking structured regions in a variety of chromatographic fractionation experiments, suggesting that this region is a large unstructured or loosely folded loop emanating from a structural domain. Both protease-sensitive regions are poorly conserved relative to the rest of the protein, and consist predominantly of polar and charged residues (Supplemental Fig. 2). Crystals were obtained using a scTel2 internal deletion mutant lacking only the first protease-sensitive region (residues 387–427).

Crystals were grown by the hanging drop vapor diffusion method at 4°C by mixing a 10 mg/mL preparation of scTel2 in 20 mM Tris-HCl, 400 mM NaCl, and 5 mM DTT (pH 8.0) with the well solution containing 0.1 M Tris-HCl, 7% (w/v) polyethylene glycol (PEG) 8000, 0.8 M NaCl, and 1.5% (v/v) ethanol (pH 8.5). Crystals of selenomethionine-substituted Tel2 were obtained in similar conditions. Crystals were cryoprotected in liquid nitrogen after brief sequential soaks in well buffer supplemented with 10%, 20%, and 30% glycerol. All data were collected at the Advanced Photon Source (APS) beamline 24ID and processed with the HKL2000 suite (Otwinowski and Minor 1997). The structure was determined using SAD with diffraction data collected at the selenium edge. The 40 selenium sites (10 per Tel2 protomer) were identified with the program SHELXD (Sheldrick 2008), and the initial phase calculation and density modification were performed with SHELXE (Sheldrick 2008). The initial phases had a mean figure of merit (f.o.m.) of 0.53–3.3 Å, with helices clearly identifiable at this stage. The noncrystallographic symmetry (ncs) operators were derived by visual inspection of the selenium sites, aided by the program SITE2RT. The approximate 2-2-2 ncs was subsequently used for averaging and density modification with the program DM (Collaborative Computational Project, Number 4 1994). The model was built with the programs O (Jones et al. 1991) and Coot (Emsley et al. 2010), and it was refined with the program REFMAC5 (Collaborative Computational Project, Number 4 1994). The refined model consists of residues 1–78, 83–370, 375–386, 428–446, 450–470, 472–553, 611–634, and 641–688 of four Tel2 protomers. There is no clear electron density for residues 79–82, 371–374, 447–449, 471, 554–610 (the second protease-susceptible region), and 635–640. We presume they are disordered. We do not have any evidence that the 2-2-2 Tel2 tetramer is physiologically relevant. The monomeric insect cell-expressed Tel2 used in crystallization does not form tetramers that can be observed by gel filtration chromatography, even at concentrations as high as 0.2 mM (data not shown). Figures were generated using PyMOL (<http://www.pymol.org>).

In vitro binding assay

Five micromolar GST or GST-tagged Tel2 was incubated with 6 μ M Tti1–Tti2 complex on ice for 10 min in 20 μ L of binding buffer consisting of 20 mM Tris-HCl, 150 mM NaCl, 5% glycerol, and 5 mM DTT (pH 8.0) prior to addition of 20 μ L of glutathione Sepharose beads. After 30 min of shaking at 4°C, the beads were spun down, and the supernatant was removed (labeled as unbound [U] fraction in Fig. 5C). The beads were washed twice with 1 mL of binding buffer, and the bound proteins were eluted in 20 μ L of binding buffer with 20 mM GSH. Ten percent of input (I) and 5 μ L of unbound (U) and bound (B) fractions were analyzed using a Coomassie-stained SDS-PAGE gel.

Acknowledgments

We thank Y. Goldgur, K. Rajashankar, and the staff of the APS 24ID beamline for help with data collection; D. White for expert mouse husbandry; the Proteomics Resource Center of Rockefeller University, and D. King of the Howard Hughes Medical Institute for help in mass spectrometry. This research was supported by a grant from the Breast Cancer Research Foundation to T.d.L., and by the Howard Hughes Medical Institute. The coordinates of scTel2 have been deposited in the RCSB Protein Data Bank with accession number 3O4Z.

References

- Abraham RT. 2004. PI 3-kinase related kinases: 'Big' players in stress-induced signaling pathways. *DNA Repair (Amst)* **3**: 883–887.
- Adami A, Garcia-Alvarez B, Arias-Palomo E, Barford D, Llorca O. 2007. Structure of TOR and its complex with KOG1. *Mol Cell* **27**: 509–516.
- Amzel LM, Huang CH, Mandelker D, Lengauer C, Gabelli SB, Vogelstein B. 2008. Structural comparisons of class I phosphoinositide 3-kinases. *Nat Rev Cancer* **8**: 665–669.
- Anderson CM, Korkin D, Smith DL, Makovets S, Seidel JJ, Sali A, Blackburn EH. 2008. Tel2 mediates activation and localization of ATM/Tel1 kinase to a double-strand break. *Genes Dev* **22**: 854–859.
- Andrade MA, Perez-Iratxeta C, Ponting CP. 2001a. Protein repeats: Structures, functions, and evolution. *J Struct Biol* **134**: 117–131.
- Andrade MA, Petosa C, O'Donoghue SI, Muller CW, Bork P. 2001b. Comparison of ARM and HEAT protein repeats. *J Mol Biol* **309**: 1–18.
- Badea TC, Wang Y, Nathans J. 2003. A noninvasive genetic/pharmacologic strategy for visualizing cell morphology and clonal relationships in the mouse. *J Neurosci* **23**: 2314–2322.
- Bakkenist CJ, Kastan MB. 2004. Initiating cellular stress responses. *Cell* **118**: 9–17.
- Ball HL, Myers JS, Cortez D. 2005. ATRIP binding to replication protein A-single-stranded DNA promotes ATR–ATRIP localization but is dispensable for Chk1 phosphorylation. *Mol Biol Cell* **16**: 2372–2381.
- Boulon S, Marmier-Gourrier N, Pradet-Balade B, Wurth L, Verheggen C, Jady BE, Rothe B, Pescia C, Robert MC, Kiss T, et al. 2008. The Hsp90 chaperone controls the biogenesis of L7Ae RNPs through conserved machinery. *J Cell Biol* **180**: 579–595.
- Branzei D, Foiani M. 2008. Regulation of DNA repair throughout the cell cycle. *Nat Rev Mol Cell Biol* **9**: 297–308.
- Cimprich KA, Cortez D. 2008. ATR: An essential regulator of genome integrity. *Nat Rev Mol Cell Biol* **9**: 616–627.
- Collaborative Computational Project, Number 4. 1994. The CCP4 suite: Programs for protein crystallography. *Acta Crystallogr D Biol Crystallogr* **50**: 760–763.
- Emsley P, Lohkamp B, Scott WG, Cowtan K. 2010. Features and development of Coot. *Acta Crystallogr D Biol Crystallogr* **66**: 486–501.
- Gano JJ, Simon JA. 2010. A proteomic investigation of ligand-dependent HSP90 complexes reveals CHORDC1 as a novel ADP-dependent HSP90-interacting protein. *Mol Cell Proteomics* **9**: 255–270.
- Garel J. 1992. Folding of large proteins: Multidomain and multisubunit proteins. In *Protein folding* (ed. TE Creighton), pp. 405–454. Freeman, New York.
- Gray PJ Jr, Prince T, Cheng J, Stevenson MA, Calderwood SK. 2008. Targeting the oncogene and kinome chaperone CDC37. *Nat Rev Cancer* **8**: 491–495.
- Guertin DA, Sabatini DM. 2007. Defining the role of mTOR in cancer. *Cancer Cell* **12**: 9–22.
- Harper JW, Elledge SJ. 2007. The DNA damage response: Ten years after. *Mol Cell* **28**: 739–745.
- Hartman PS, Herman RK. 1982. Radiation-sensitive mutants of *Caenorhabditis elegans*. *Genetics* **102**: 159–178.
- Hayashi T, Hatanaka M, Nagao K, Nakaseko Y, Kanoh J, Kokubu A, Ebe M, Yanagida M. 2007. Rapamycin sensitivity of the *Schizosaccharomyces pombe* tor2 mutant and organization of two highly phosphorylated TOR complexes by specific and common subunits. *Genes Cells* **12**: 1357–1370.
- Holm L, Kaariainen S, Rosenstrom P, Schenkel A. 2008. Searching protein structure databases with DaliLite v.3. *Bioinformatics* **24**: 2780–2781.
- Huen J, Kakihara Y, Ugwu F, Cheung KL, Ortega J, Houry WA. 2010. Rvb1–Rvb2: Essential ATP-dependent helicases for critical complexes. *Biochem Cell Biol* **88**: 29–40.
- Izumi N, Yamashita A, Iwamatsu A, Kurata R, Nakamura H, Saari B, Hirano H, Anderson P, Ohno S. 2010. AAA⁺ proteins RUVBL1 and RUVBL2 coordinate PIKK activity and function in nonsense-mediated mRNA decay. *Sci Signal* **3**: ra27. doi: 10.1126/scisignal.2000468.
- Jeronimo C, Forget D, Bouchard A, Li Q, Chua G, Poitras C, Therien C, Bergeron D, Bourassa S, Greenblatt J, et al. 2007. Systematic analysis of the protein interaction network for the human transcription machinery reveals the identity of the 7SK capping enzyme. *Mol Cell* **27**: 262–274.
- Jha S, Dutta A. 2009. RVB1/RVB2: Running rings around molecular biology. *Mol Cell* **34**: 521–533.
- Jones TA, Zou JY, Cowan SW, Kjeldgaard M. 1991. Improved methods for building protein models in electron density maps and the location of errors in these models. *Acta Crystallogr A* **47**: 110–119.
- Kaizuka T, Hara T, Oshiro N, Kikkawa U, Yonezawa K, Takehana K, Iemura S, Natsume T, Mizushima N. 2010. Tti1 and Tel2 are critical factors in mammalian target of rapamycin complex assembly. *J Biol Chem* **285**: 20109–20116.
- Kim DH, Sarbassov DD, Ali SM, King JE, Latek RR, Erdjument-Bromage H, Tempst P, Sabatini DM. 2002. mTOR interacts with raptor to form a nutrient-sensitive complex that signals to the cell growth machinery. *Cell* **110**: 163–175.
- Lakowski B, Hekimi S. 1996. Determination of life-span in *Caenorhabditis elegans* by four clock genes. *Science* **272**: 1010–1013.
- Laplante M, Sabatini DM. 2009. mTOR signaling at a glance. *J Cell Sci* **122**: 3589–3594.
- Llorca O, Rivera-Calzada A, Grantham J, Willison KR. 2003. Electron microscopy and 3D reconstructions reveal that human ATM kinase uses an arm-like domain to clamp around double-stranded DNA. *Oncogene* **22**: 3867–3874.

Takai et al.

- Lustig AJ, Petes TD. 1986. Identification of yeast mutants with altered telomere structure. *Proc Natl Acad Sci* **83**: 1398–1402.
- Ma XM, Blenis J. 2009. Molecular mechanisms of mTOR-mediated translational control. *Nat Rev Mol Cell Biol* **10**: 307–318.
- Murr R, Vaissiere T, Sawan C, Shukla V, Herceg Z. 2007. Orchestration of chromatin-based processes: Mind the TRRAP. *Oncogene* **26**: 5358–5372.
- Nicholson P, Yepiskoposyan H, Metze S, Zamudio Orozco R, Kleinschmidt N, Muhlemann O. 2010. Nonsense-mediated mRNA decay in human cells: Mechanistic insights, functions beyond quality control and the double-life of NMD factors. *Cell Mol Life Sci* **67**: 677–700.
- Ohji G, Hidayat S, Nakashima A, Tokunaga C, Oshiro N, Yoshino K, Yokono K, Kikkawa U, Yonezawa K. 2006. Suppression of the mTOR–raptor signaling pathway by the inhibitor of heat shock protein 90 geldanamycin. *J Biochem* **139**: 129–135.
- Otwinowski Z, Minor W. 1997. Processing of X-ray diffraction data collected in oscillation mode. *Methods Enzymol* **276**: 307–326.
- Ren X, Hurley JH. 2010. VHS domains of ESCRT-0 cooperate in high-avidity binding to polyubiquitinated cargo. *EMBO J* **29**: 1045–1054.
- Sarbasov DD, Ali SM, Sengupta S, Sheen JH, Hsu PP, Bagley AF, Markhard AL, Sabatini DM. 2006. Prolonged rapamycin treatment inhibits mTORC2 assembly and Akt/PKB. *Mol Cell* **22**: 159–168.
- Sheldrick GM. 2008. A short history of SHELX. *Acta Crystallogr A* **64**: 112–122.
- Shevchenko A, Roguev A, Schaft D, Buchanan L, Habermann B, Sakalar C, Thomas H, Krogan NJ, Stewart AF. 2008. Chromatin central: Towards the comparative proteome by accurate mapping of the yeast proteomic environment. *Genome Biol* **9**: R167. doi: 10.1186/gb-2008-9-11-r167.
- Shikata M, Ishikawa F, Kanoh J. 2007. Tel2 is required for activation of the Mrc1-mediated replication checkpoint. *J Biol Chem* **282**: 5346–5355.
- Shiloh Y. 2003. ATM and related protein kinases: Safeguarding genome integrity. *Nat Rev Cancer* **3**: 155–168.
- Sibanda BL, Chirgadze DY, Blundell TL. 2009. Crystal structure of DNA-PKcs reveals a large open-ring cradle comprised of HEAT repeats. *Nature* **463**: 118–121.
- Takai H, Wang RC, Takai KK, Yang H, de Lange T. 2007. Tel2 regulates the stability of PI3K-related protein kinases. *Cell* **131**: 1248–1259.
- Te J, Jia L, Rogers J, Miller A, Hartson SD. 2007. Novel subunits of the mammalian Hsp90 signal transduction chaperone. *J Proteome Res* **6**: 1963–1973.
- Wandinger SK, Richter K, Buchner J. 2008. The Hsp90 chaperone machinery. *J Biol Chem* **283**: 18473–18477.
- Whitesell L, Lindquist SL. 2005. HSP90 and the chaperoning of cancer. *Nat Rev Cancer* **5**: 761–772.
- Young JC, Moarefi I, Hartl FU. 2001. Hsp90: A specialized but essential protein-folding tool. *J Cell Biol* **154**: 267–273.
- Zou L, Elledge SJ. 2003. Sensing DNA damage through ATRIP recognition of RPA–ssDNA complexes. *Science* **300**: 1542–1548.